Journal of Colloid and Interface Science **245,** 68–74 (2002)
doi:10.1006/jcis.2001.7999, available online at http://www.idealibrary.com on IDEAL®

Characterization of Nanostructured Hollow Polymer Spheres with Small-Angle Neutron Scattering (SANS)

C. A. McKelvey and E. W. Kaler[1]

University of Delaware, Department of Chemical Engineering, Center for Molecular Engineering and Thermodynamics, Newark, Delaware 19716

Received February 20, 2001; accepted October 1, 2001; published online November 14, 2001

Hollow polymer spheres synthesized from a vesicle-directed polymerization can be dried and redispersed in water using a variety of nonionic ethoxylated alcohol surfactants as stabilizers. The final dispersions consist of both polymer shells and surfactant micelles, which remain together in colloidal suspension for at least several months. Small-angle neutron scattering (SANS) is used to measure the polymer shell thickness (63 Å) and core radius (560 Å) of the surfactant-stabilized hollow polymer spheres in the presence of surfactant micelles. Characterization by SANS provides information about the surfactant bilayer and polymer shell thicknesses which were previously unattainable. © 2002 Elsevier Science

Key Words: **small-angle neutron scattering; vesicle; polymerization; nanostructured particles; templating.**

INTRODUCTION

Submicron hollow spheres are potentially useful in a variety of applications ranging from catalysis to controlled release (1). Their large surface area and ability to compartmentalize the aqueous domain on small length scales make these particles particularly attractive.

We have shown that hollow cross-linked polystyrene spheres can be templated from equilibrium vesicle phases (2), as outlined in Fig. 1. Divinyl benzene, a hydrophobic monomer, swells the bilayers in an equilibrium vesicle phase. Free radical polymerization locks in the microstructure of the vesicle template in a morphosynthetic process where the monomer and its subsequent polymeric product appear confined to the vesicle bilayer. The hollow polymer spheres are typically isolated by dialysis in methanol and completely dried. The hollow polymer morphology is quite different from the structures obtained by others for the polymerization of styrene and divinyl benzene in different surfactant vesicles (3).

Resuspension of these hydrophobic particles in water is possible after appropriate functionalization of the surface. Both sulfonation and adsorption of nonionic surfactant allow the hollow spheres to be redispersed (2). Sulfonating the polymer surface creates an electrostatic repulsion between the particles that induces stabilization. Nonionic surfactants promote stability through steric repulsion between the hydrophilic groups of adsorbed surfactant monolayers. A schematic of a surfactant-stabilized polymer shell is shown in Fig. 2, along with the two primary-length scales of shell thickness and particle diameter.

Ethoxylated alcohol surfactants were chosen to stabilize the hollow polymer spheres in water because their hydrophobic and hydrophilic character can be adjusted systematically. Ethoxylated alcohol surfactants have the general formula, $CH_3(CH_2)_{i-1}(OCH_2CH_2)_jOH$, and are often referred to as C_iE_j's where "i" denotes the number of carbon atoms in the hydrophobic tail and "j" denotes the number of ethoxylate groups in the hydrophilic head. We previously reported (2) the use of $C_{12}E_8$ for resuspension of these hollow polymer spheres, but it is of interest to study the effect of changing the surfactant architecture on the particle stability. In particular, we report the application here of $C_{12}E_8$, $C_{12}E_{23}$, $C_{16}E_{20}$, and $C_{18}E_{20}$ to produce stable aqueous dispersions of the polymer shells. The suspended particles were characterized by small-angle neutron scattering (SANS), which is a useful tool because both the shell thickness and particle diameter are in the range of 10 to 1000 Å.

Micelles are present in the surfactant-stabilized dispersions because the critical micelle concentrations (CMCs) of these surfactants are low (ca. $5–10 \times 10^{-5}$ M) (4–6). Globular micelles are expected to form in the C_iE_j solutions at ambient temperatures for the concentration ranges explored here (7, 8). The presence of micelles complicates the characterization of the surfactant-stabilized hollow spheres with SANS, although SANS has been successfully used to characterize a variety of solid particles covered with adsorbed surfactant monolayers (9–14).

Because the samples of interest contain polydisperse populations of both hollow particles and micelles, the scattered intensity is usefully discussed in terms of a p-component mixture of particles with different sizes (15):

$$I(q) = \sum_{i}^{p}\sum_{j}^{p} \sqrt{n_i n_j}\, f_i(q)\, f_j(q) S_{ij}(q). \qquad [1]$$

[1] To whom correspondence should be addressed at College of Engineering, University of Delaware, Newark, DE 19716. Fax: (302)831-6751. E-mail: Kaler@che.udel.edu.

0021-9797/02 $35.00

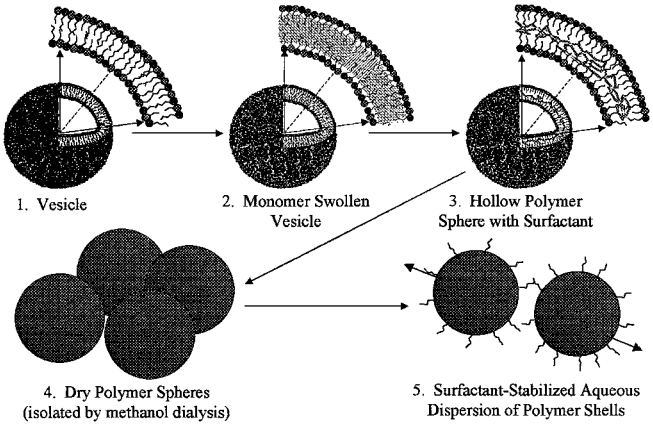

FIG. 1. Schematic summary of catanionic vesicle-directed synthesis of hollow polymer spheres described in Ref. (2).

The particles of each indexed size are described by a number density, n, scattering amplitude, f, and partial structure factors, S. The geometries of these structures are illustrated in Fig. 2.

The scattering intensity is a function of the wave vector, q, which in turn depends on the wavelength of neutrons, λ, and the angle of scattering, θ:

$$q = \left(\frac{4\pi}{\lambda}\right)\sin\left(\frac{\theta}{2}\right). \qquad [2]$$

Nonionic micelles are typically modeled as spheres with a constant contrast or as a hydrocarbon core with a hydrophilic shell, each with their own respective contrasts. The micelle scattering observed here was adequately described by either model, so the simpler constant contrast model was implemented. The scattering amplitude, $f(q)$, for a spherical micelle is

$$f_{\text{micelle}} = 3\Delta\rho V_{\text{m}}\frac{j_1(qR)}{qR}, \qquad [3]$$

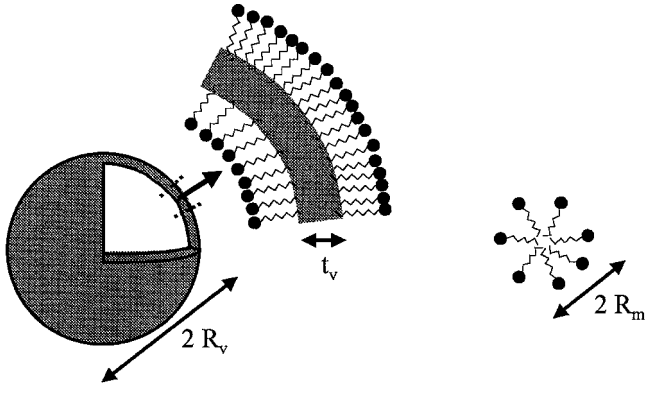

FIG. 2. Hollow polymer sphere with adsorbed surfactant layers (left) and a micelle (right) showing appropriate model dimensions for each.

where $\Delta\rho$ is the scattering contrast, V_{m} is the micelle volume, R is the radius, and $j_1(x) = [\sin(x) - x\cos(x)]/x^2$.

The geometry used to represent surfactant-stabilized polymer shells consists of an aqueous core surrounded by the polymer layer and two surfactant monolayers (Fig. 2). For this geometry, the scattering amplitude is

$$f_{\text{p}} = 3(\rho_0 - \rho_1)V_0\frac{j_1(qR_0)}{qR_0} + 3(\rho_1 - \rho_2)V_1\frac{j_1(qR_1)}{qR_1} + 3(\rho_2 - \rho_3)V_2\frac{j_1(qR_2)}{qR_2} + 3(\rho_3 - \rho_4)V_3\frac{j_1(qR_3)}{qR_3}. \qquad [4]$$

The indices 0 through 4 designate the radii and scattering length densities of the core, inner surfactant shell, polymer layer, outer surfactant shell, and solvent, respectively.

The partial structure factors, S_{ij}'s, in Eq. [1] can be calculated analytically by using a hard-sphere interaction to describe the interparticle potential and the Percus-Yevick closure relationship in order to solve the Ornstein-Zernicke equation. Expressions for the partial structure factors under these conditions have been determined by Vrij for polydisperse populations of Schulz distributed spheres (16).

The bimodal distribution of the outer diameters of the surfactant micelles and hollow polymer particles was modeled using two separate Schulz distributions. The scattering amplitudes and partial structure factors were determined for the micelles and polymer shells from each distribution so that the scattered intensity could be calculated (Eq. [1]). Several parameters are required in order to calculate values of the scattered intensity from Eq. [1] and these parameters were obtained by fitting experimental SANS data with this "bimodal" model and adjusting the model parameters until the value of χ^2 was minimized.

The micelles are described by their average radius (R_{m}), polydispersity (P_{m}), and density (ρ_{m}). These parameters were obtained in separate experiments wherein the scattering from micellar surfactant solutions was evaluated in the absence of polymer shells.

The structure of the hollow polymer particles is also described by three parameters: the average core radius (R_{v}), polymer shell thickness (t_{v}), and polydispersity (P_{v}). The polydispersity in this case applies to both the core and the shells because the ratio of the core radius to each shell thickness is held constant. Calculation of the excluded volume interaction needed for the structure factor is based on the outermost radius (i.e., the core radius plus shell thicknesses). The thickness of the adsorbed monolayers on the polymer shells was set equal to the radius of the micelle formed by the given surfactant. The density of cross-linked polystyrene was assumed to be 1.1 g/cc. The final parameter needed is the fraction of C_iE_j adsorbed on the hollow polymer shells, f. This parameter describes the partitioning of the surfactant between micelles and its adsorption on the polymer shells.

MATERIALS AND METHODS

Octa-ethyleneglycol mono *n*-dodecyl ether ($C_{12}E_8$) was purchased from Nikko Chemicals Co. (Tokyo, Japan). Brij 35 ($\sim C_{12}E_{23}$), Brij 58 ($\sim C_{16}E_{20}$), and Brij 78 ($\sim C_{18}E_{20}$) were purchased from Aldrich. D_2O (99.9%) was obtained from Cambridge Isotopes. All materials were used as received. The synthesis and materials used to make the hollow polymer spheres are described elsewhere (2).

To resuspend the polymer shells, 10 g of the C_iE_j solution in D_2O was added to the dry polymer powder in a 20-ml scintillation vial. Although stable dispersions of the polymer shells can be formed by shaking the $C_{12}E_8$ solution with the polymer particles, sonication is generally required to produce stable solutions with the impure Brij surfactants. All of the samples were sonicated for 15 min in an ice bath using a Heat Systems Ultrasonics Model W-225 sonicator. The mixtures were then centrifuged for 3 h at 25°C and the supernatant was removed for SANS characterization.

The SANS measurements were made at the National Institute of Standards and Technology (NIST) in Gaithersburg, MD. An average radiation wavelength of 6 Å with a spread of 11% was used. Samples were held at 25°C in quartz "banjo" cells with 1-mm path lengths. Three sample-detector distances were used to give a range in scattering vector of 0.005 to 0.5 $Å^{-1}$. The data were corrected for detector efficiency, background, and empty cell scattering before placement on an absolute scale using NIST procedures.

RESULTS

The three model parameters for $C_{12}E_8$ micelles were fit by simultaneously minimizing the average value of χ^2 for three spectra (Fig. 3). The fitted radius, polydispersity, and density were 26.2 Å, 0.14, and 1.38 g/cc, respectively (the surfactant density was incorrectly calculated in a previous paper as 0.92 g/cc) (2). These parameters were held fixed and incorporated in the model used to fit the scattering from surfactant-stabilized polymer shells. The scattering length density of $C_{12}E_8$ is 2.4×10^{-7} $Å^{-2}$ (see appendix). Table 1 summarizes the modeling results for all the SANS spectra.

The bimodal scattering model was fit to SANS spectra from various concentrations of $C_{12}E_8$-stabilized polymer shells by minimizing the average value of χ^2 for four spectra (Fig. 4). The fitted core radius, polymer thickness, polydispersity, and fraction of $C_{12}E_8$ adsorbed were 560 Å, 63 Å, 0.39, and 0.50, respectively. The calculated scattering length density of the polymer is 1.5×10^{-6} $Å^{-2}$ (see appendix). From the fitted dimensions and the measured weight of the polymer in each sample the excluded volume fractions of the polymer shells were calculated as 4.1, 6.7, and 9.4% for the 0.15, 0.25, and 0.35% weight

TABLE 1
Summary of Adjustable Parameters Used for the SANS Modeling

	Micelle model			Hollow polymer sphere model			
Surfactant	R_m (Å)	Poly.	Density (g/cc)	R_v (Å)	t_v (Å)	Poly.	f
$C_{12}E_8$	26.2	0.14	1.38	560	63	0.39	0.50
$C_{12}E_{23}$	26.8	0.23	2.37	560	63	0.39	0.55
$C_{16}E_{20}$	31.4	0.18	1.80	560	63	0.39	0.40
$C_{18}E_{20}$	34.4	0.17	1.61	560	63	0.39	0.65

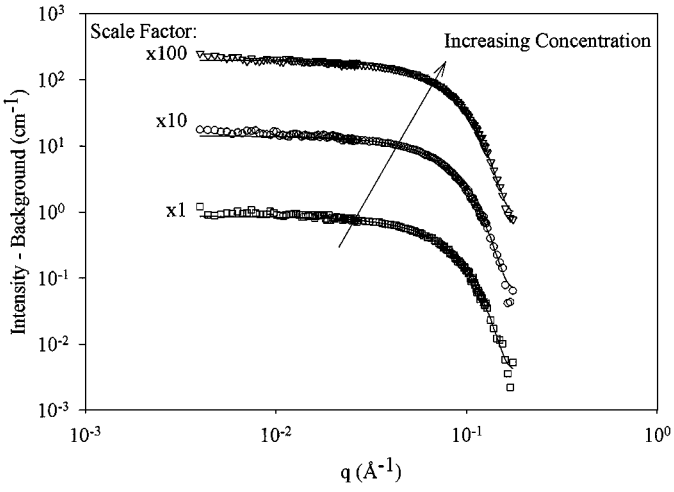

FIG. 3. SANS data $I - B$ (intensity minus background) versus q, for the $C_{12}E_8$ micelles in D_2O. Open symbols are the data for 0.3 wt% $C_{12}E_8$ (□), 0.5 wt% $C_{12}E_8$ (○), 0.7 wt% $C_{12}E_8$ (▽). The solid lines are the polydisperse hard-sphere model simultaneously fit to all three spectra using three adjustable parameters: 26.2 Å radius, 0.14 polydispersity, and a density of 1.38 g/cc. The data are offset by the scale factors shown for clarity.

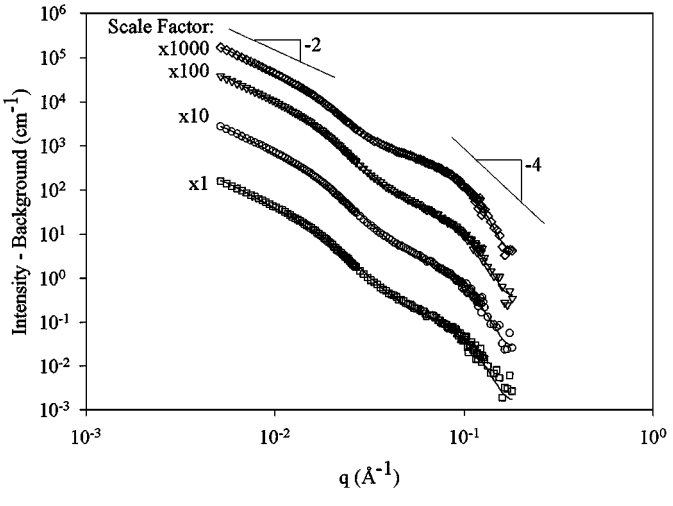

FIG. 4. SANS data, $I - B$ versus q, for the $C_{12}E_8$-stabilized hollow polymer spheres in D_2O. Open symbols are the data for 0.15 wt% $C_{12}E_8$ and 0.15 wt% polymer (□), 0.25 wt% $C_{12}E_8$ and 0.25 wt% polymer (○), 0.35 wt% $C_{12}E_8$ and 0.35 wt% polymer (▽), and 0.35 wt% $C_{12}E_8$ and 0.15 wt% polymer (◇). The solid lines are the polydisperse multiple shell model discussed in the text with four fitted parameters: 560 Å core radius, 63 Å polymer shell thickness, 0.39 polydispersity, and a fraction of $C_{12}E_8$ adsorbed of 0.5. The data are offset by the scale factors shown for clarity.

fraction solutions, respectively. The area per headgroup of adsorbed surfactant (30 Å^2/molecule) can be calculated from the fraction of C_iE_j adsorbed, f. The same bimodal model was then used to fit SANS spectra from $C_{12}E_{23}$, $C_{16}E_{20}$, and $C_{18}E_{20}$-stabilized hollow spheres by only adjusting the fraction of C_iE_j adsorbed. The core radius, polymer thickness, and polydispersity were fixed at 560 Å, 63 Å, and 0.39, respectively, since these should only depend on the structure of the polymer shells themselves and not the type of surfactant chosen. In each case, micellar scattering spectra are again needed to obtain the micelle scattering parameters (radius, polydispersity, and density) used in the bimodal model.

Two $C_{12}E_{23}$ SANS spectra, one with micelles only and one with hollow polymer spheres and micelles, were fit separately by minimizing χ^2 (Fig. 5). The radius, polydispersity, and density obtained from the micellar model fit were 26.8 Å, 0.23, and 2.37 g/cc. The fraction of C_iE_j adsorbed used to fit the bimodal model to the hollow sphere spectrum was 0.55, corresponding to an adsorbed surfactant headgroup area of 60 Å^2/molecule. The scattering length density of the surfactant used was 4.4×10^{-7} Å^{-2} (see appendix).

Finally, the effect of the surfactant tail-group length can be determined by comparing the results for $C_{16}E_{20}$ and $C_{18}E_{20}$. Again two spectra, one with micelles only and one with polymer shells and micelles, were fit separately by minimizing χ^2 (Figs. 6 and 7). The radius, polydispersity, and density from the micellar models of $C_{16}E_{20}$ and $C_{18}E_{20}$ were 31.4 Å, 0.18, and 1.80 g/cc and 34.4 Å, 0.17, and 1.61 g/cc, respectively. The fractions of surfactant adsorbed for $C_{16}E_{20}$ and $C_{18}E_{20}$ were 0.40 and 0.65 corresponding to adsorbed surfactant headgroup areas of 70 and 50 Å^2/molecule. Scattering length densities used for $C_{16}E_{20}$ and $C_{18}E_{20}$ were 3.8×10^{-7} and 3.6×10^{-7} Å^{-2} (see appendix).

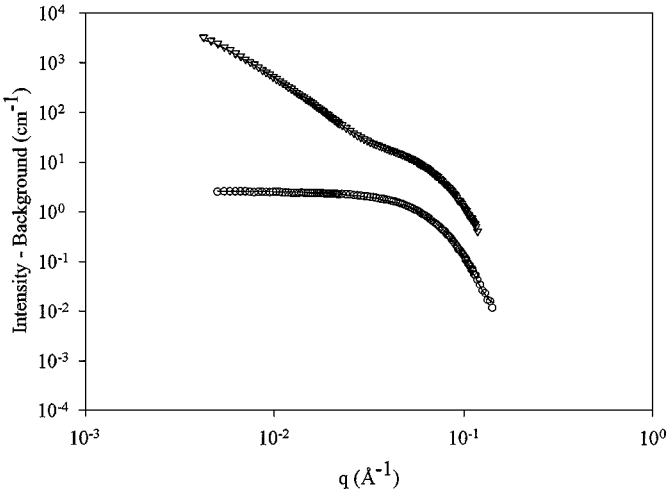

FIG. 6. SANS data, $I - B$ versus q, for the $C_{16}E_{20}$ micelles and $C_{16}E_{20}$-stabilized hollow polymer spheres in D_2O. Open symbols are the data for 0.65 wt% $C_{16}E_{20}$ (○), and for 0.65 wt% $C_{16}E_{20}$, with 0.15 wt% polymer (▽). The solid line through the micellar spectrum is a polydisperse hard-sphere model with three adjustable parameters: 31.4 Å radius, 0.18 polydispersity, and a density of 1.80 g/cc. The solid line through the hollow polymer sphere spectrum is the polydisperse multiple shell model discussed in the text. Here only the fraction of $C_{12}E_{23}$ adsorbed (0.40) is adjustable. The data are offset by a scale factor of 10 for clarity.

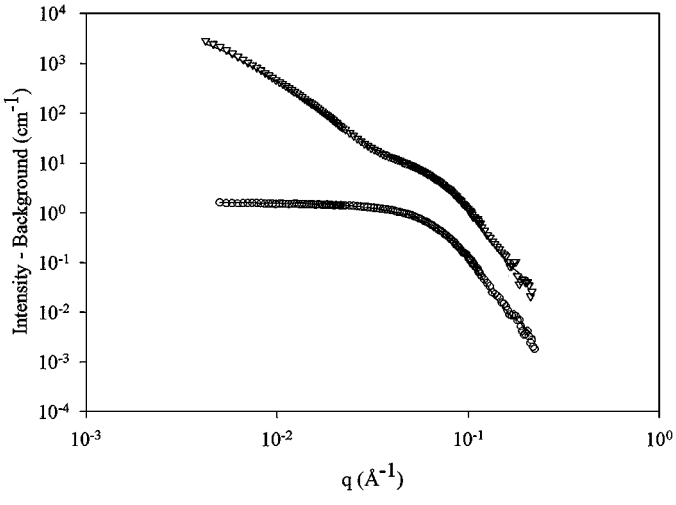

FIG. 5. SANS data, $I - B$ versus q, for the $C_{12}E_{23}$ micelles and $C_{12}E_{23}$-stabilized hollow polymer spheres in D_2O. Open symbols are the data for 0.7 wt% $C_{12}E_{23}$ (○), and for 0.7 wt% $C_{12}E_{23}$, with 0.15 wt% polymer (▽). The solid line through the micellar spectrum is a polydisperse hard-sphere model with three adjustable parameters: 26.8 Å radius, 0.23 polydispersity, and a density of 2.37 g/cc. The solid line through the hollow polymer sphere spectrum is the polydisperse multiple shell model discussed in the text. Here only the fraction of $C_{12}E_{23}$ adsorbed (0.55) is adjustable. The data are offset by a scale factor of 10 for clarity.

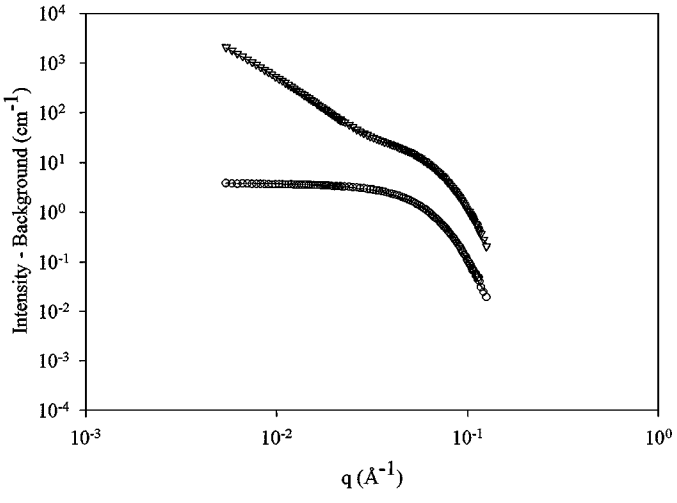

FIG. 7. SANS data, $I - B$ versus q, for the $C_{18}E_{20}$ micelles and $C_{18}E_{20}$-stabilized hollow polymer spheres in D_2O. Open symbols are the data for 0.67 wt% $C_{18}E_{20}$ (○), and for 0.67 wt% $C_{18}E_{20}$, with 0.15 wt% polymer (▽). The solid line through the micellar spectrum is a polydisperse hard-sphere model with three adjustable parameters: 34.4 Å radius, 0.17 polydispersity, and a density of 1.61 g/cc. The solid line through the hollow polymer sphere spectrum is the polydisperse multiple shell model discussed in the text. Here only the fraction of $C_{12}E_{23}$ adsorbed (0.65) is adjustable. The data are offset by a scale factor of 10 for clarity.

DISCUSSION

Several groups have characterized $C_{12}E_8$ micelles with SANS and obtained radii of 32, 36, and 30 Å (8, 17, 18). These values are slightly larger than the value of 26 Å reported here and may be explained by the higher concentrations used in the other studies. Schefer *et al*. (19) reports a radius of gyration for $C_{16}E_{20}$ of 32 Å from SANS, which is larger than the value of 24 Å for the radius of gyration here ($R_g = 0.77 \times R_0$) (20). Other studies of micellar size with quasielastic light scattering (QELS) (21) and optical probes (22) generally found radii ca. 1.5–2 times larger than those from SANS, probably because of the differences in the treatment of polydispersity and hydrodynamic effects.

The bimodal model captured the characteristics of a variety of spectra involving different particle concentrations and surfactant types. The core radius of the polymer shells extracted from the model fits was 560 Å in comparison to a 600 Å radius previously measured using QELS (2). A slightly larger size is expected for QELS measurements since the SANS model radius is the core dimension of the polymer shells while QELS measures the hydrodynamic radius. Furthermore, the error in the model fits (χ^2) to the SANS spectra obtained from the polymer shell dispersions did not strongly depend on the value of the core radius. Table 2 is a summary of the ranges of parameter values that cause up to a 5% change in the minimum χ^2 values. The dependence of χ^2 on much larger core radii values was particularly weak, suggesting that SANS is not the most accurate method to determine the diameter of such polydisperse spheres.

Independent measurement of the polymer shell thickness, t_v, is not available. This parameter is required to calculate the excluded volume fraction of the hollow particles from the known mass of the particles in a given sample. A mass balance incorporating the density of the polymer, particle radius, particle polydispersity, and shell thickness is used to calculate the excluded volume fraction, and the overall fit is sensitive to the value of t_v, in contrast to the value of the core radius. Changes in the value of t_v had a dramatic impact on the shape of the SANS model.

An interesting feature of the scattering from equilibrium vesicles (23) and these polymer shells is a q^{-2} dependence of the scattered intensity at smaller q values (Figs. 4 and 8). This occurs when the shell thickness is much smaller than the D_2O core of the scatterer (i.e., $t < R_v$). The shell scattering is then identical to that of an extended sheet (24). The q^{-2} region of an equilibrium vesicle SANS spectrum covers larger q values than a SANS spectrum from surfactant-stabilized polymer spheres (Fig. 8). The higher q limit of the q^{-2} dependence in the scattered intensity varies inversely with the overall thickness of the hollow shell. The surfactant-stabilized polymer particles have thicker shells than the equilibrium vesicles since they contain an additional polymer layer. This thicker shell results in a drop-off of the q^{-2}-dependent region at lower q values (see arrows in Fig. 8).

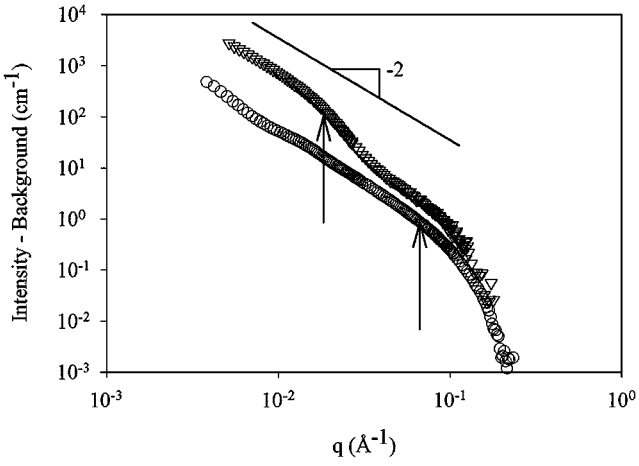

FIG. 8. Comparison of SANS spectra from catanionic vesicles (0.7 wt% CTAT and 0.3 wt% SDBS, ○) and $C_{12}E_8$-stabilized hollow polymer spheres (0.15 wt% $C_{12}E_8$ and 0.15 wt% polymer, ▽). Note the q^{-2} dependence of both spectra at lower q values as indicated by the straight reference line. The arrows indicate the high-q boundary of the q^{-2} region for each spectrum.

At even higher q values, the SANS spectra for each of the surfactant-stabilized polymer shell dispersions drops off at a rate greater than q^{-4}, which is indicative of diffuse Porod limit scattering (Fig. 4) (25). This suggests that the interfaces of the polymer shell are diffuse, much like the case for catanionic vesicles (23), diffuse polymer interfaces (26, 27), and $C_{12}E_5$ bilayers (25).

In the fitting of the bimodal model presented here, the core of the hollow spheres is assumed to be D_2O. During the fabrication process, the hollow spheres are filled with H_2O before drying. If the cores of the dry particles are empty, then D_2O should fill them

TABLE 2
Model Parameter Values Corresponding to a 5% Increase in the Minimum χ^2 Value

	Micelle model			Hollow polymer sphere model			
Surfactant	R_m (Å)	Polydispersity	Density (g/cc)	R_v (Å)	t_v (Å)	Polydispersity	f
$C_{12}E_8$	26.1–26.3	0.14–0.15	1.38–1.39	550–585	60–65	0.38–0.41	0.46–0.55
$C_{12}E_{23}$	26.7–26.9	0.23–0.23	2.35–2.38	550–585	60–65	0.38–0.41	0.47–0.64
$C_{16}E_{20}$	31.3–31.5	0.17–0.18	1.65–1.81	550–585	60–65	0.38–0.41	0.40–0.41
$C_{18}E_{20}$	34.4–34.5	0.17–0.17	1.60–1.62	550–585	60–65	0.38–0.41	0.64–0.66

when they are resuspended. On the other hand, if the polymer shell is impermeable to water, the composition of the core would be unknown. SANS spectra from polymer shells could not be fit using the same bimodal model with the assumption that the cores were filled with H_2O instead of D_2O, suggesting the polymer shells are indeed permeable to water.

The model also describes one monolayer of surfactant adsorbed to each side of the polymer shell (Fig. 2), again under the assumption that the polymer layer is permeable. If the polymer shell is impermeable to surfactants, then no C_iE_j could penetrate the inside of the hollow shells, but instead a surfactant monolayer from the initial catanionic vesicle templating process (Fig. 1) would be trapped inside. A similar bimodal model that incorporated only one surfactant monolayer on the outer surface of the polymer shells could also successfully fit the observed SANS spectra. The only difference in the fitted parameters obtained using this single surfactant monolayer model is an increase the polymer shell thickness, but the overall shell thickness (polymer and all surfactant layers) is unchanged. Thus these SANS experiments alone cannot conclusively determine the exact composition of the polymer shells, although contrast variation experiments could be used to examine the polymer shell and the adsorbed surfactant layers independently.

It is clear that a hollow structure exists due to both the success of modeling the SANS spectra with a core-shell geometry and the q^{-2} dependence of the spectra at lower q values. This compliments cryogenic transmission electron microscopy pictures which clearly depict hollow structures in dispersions of the hollow particles stabilized with $C_{12}E_8$ (2).

The Brij surfactants are the most efficient surfactants on a molar basis in dispersing hollow polymer spheres, and stabilization could be achieved with less adsorbed surfactant than for the $C_{12}E_8$ surfactant. The Brij surfactants used all have significantly longer head groups than $C_{12}E_8$, and such head groups would be more effective at sterically stabilizing the hydrophobic particles. Because the Brij surfactants are mixtures with varying head-group lengths, the polydispersity of the head groups could also play a role in the enhanced stability.

SUMMARY

The scattering from hollow cross-linked polystyrene spheres stabilized by C_iE_j surfactants was successfully modeled by accounting for scattering from both micelles and polymer shells containing adsorbed surfactant. These models yield a core diameter of 560 Å and a polymer shell thickness of 63 Å. The SANS spectra confirm that the polymer particles are hollow due to the characteristic q^{-2} behavior observed and the successful fit of a core-shell model of the SANS data.

The modeling could not distinguish the number of adsorbed surfactant monolayers, although both an inner and outer monolayer should be present as a result of either the synthesis or stabilization procedure.

APPENDIX

Scattering length densities (SLDs) can be calculated from the following equation,

$$\mathrm{SLD} = \frac{\sum_i b_i}{\sum_i v_i},$$

where "i" is an index for each atom of the molecule, b_i is the scattering amplitude of the i-th atom, and v_i is the volume of the i-th atom. The values of b_i and v_i have been tabulated for many atoms (28). For carbon, hydrogen, and oxygen the scattering amplitudes are 0.665×10^{-4}, -0.374×10^{-4}, and 0.580×10^{-4} Å, respectively. Molecular volume can be calculated from the density of a given substance. The densities used for $C_{12}E_8$, $C_{12}E_{23}$, $C_{16}E_{20}$, $C_{18}E_{20}$, and the polymer were 0.99, 1.06, 1.04, 1.04, and 1.10 g/cc. From these densities molecular volumes of 900, 1900, 1800, 1800, and 200 $Å^3$ were calculated. The scattering length densities are then 2.4×10^{-7}, 4.4×10^{-7}, $3. \times 10^{-7}$, 3.6×10^{-7}, and 1.5×10^{-6} $Å^{-2}$, respectively. The scattering length density of D_2O used for all calculations was 6.3×10^{-6} $Å^{-2}$.

Background intensities for each spectrum were obtained from the slope of a Porod plot ($I \times q^{-4}$ versus q^{-4}). These values were subtracted from the raw scattered intensity to correct for background scattering prior to modeling.

ACKNOWLEDGMENTS

The authors thank Carlos C. Co for supplying the code used to calculate the partial structure factors. This work was supported by NASA Grant NAG3-1955 and NSF CTS-9814399. We acknowledge the support of the National Institute of Standards and Technology, U.S. Department of Commerce, in providing facilities used in this work.

REFERENCES

1. Lasic, D. D., "Liposomes: From Physics to Applications." Elsevier, New York, 1993.
2. McKelvey, C. A., Kaler, E. W., Coldren, B., Jung, H.-T., and Zasadzinski, J. A., *Langmuir* **16,** 8285 (2000).
3. Jung, M., Hubert, D. H. W., Bomans, P. H. H., Frederik, P. M., Meuldijk, J., van Herk, A. M., Fischer, H., and German, A. L., *Langmuir* **13,** 6877 (1997).
4. Elworthy, P. H., and MacFarlane, C. B., *J. Pharm. Pharmacol*. **14,** 100 (1962).
5. Becher, P., *J. Phys. Chem*. **63,** 1675 (1959).
6. Ross, S., and Olivier, J. P., *J. Phys. Chem*. **63,** 1671 (1959).
7. Triolo, R., Magid, L. J., Johnson, J. S., and Child, H. R., *J. Phys. Chem*. **86,** 3689 (1982).
8. Corti, M., Degiorgio, V., Hayter, J. B., and Zulauf, M., *Chem. Phys. Lett*. **109,** 579 (1984).
9. Markovic, I., Ottewill, R. H., Cebula, D. J., Field, I., and Marsh, J. F., *Colloid Polym. Sci*. **262,** 648 (1984).
10. Markovic, I., and Ottewill, R. H., *Colloid Polym. Sci*. **264,** 65 (1986).
11. Markovic, I., and Ottewill, R. H., *Colloid Polym. Sci*. **264,** 454 (1986).
12. Cummins, P. G., Staples, E., and Penfold, J., *J. Phys. Chem*. **94,** 3740 (1990).
13. Cummins, P. G., Staples, E., and Penfold, J., *J. Phys. Chem*. **95,** 5902 (1991).

14. Harris, N. M., Ottewill, R. H., and White, J. W., "Determination of the Adsorption of Surface Active Agents on Latex Particles by Small Angle Neutron Scattering." Plenum, London, 1983.
15. Guiner, A., and Fournet, G., "Small Angle Scattering of X-Rays." Wiley, New York, 1955.
16. Vrij, A., *J. Chem. Phys*. **71,** 3267 (1979).
17. Tanford, C., Nozaki, Y., and Rohde, M. F., *J. Phys. Chem*. **81,** 1555 (1977).
18. Magid, L. J., Triolo, R., and Johnson, J. S., *J. Phys. Chem*. **88,** 5730 (1984).
19. Schefer, J., McDaniel, R., and Schoenborn, B. P., *J. Phys. Chem*. **92,** 729 (1988).
20. Porod, G., *in* "Small Angle X-Ray Scattering" (O. Glatter and O. Kratky, Eds.), p. 26. Academic Press, London, 1982.
21. Becher, P., *J. Colloid Sci*. **16,** 49 (1961).
22. Phillies, G. D. J., Hunt, R. H., Strang, K., and Sushkin, N., *Langmuir* **11,** 3408 (1995).
23. Brasher, L. L., and Kaler, E. W., *Langmuir* **12,** 6270 (1996).
24. Porod, G., *in* "Small Angle X-Ray Scattering" (O. Glatter and O. Kratky, Eds.), p. 17. Academic Press, London, 1982.
25. Strey, R., Winkler, J., and Magid, L., *J. Phys. Chem*. **95,** 7502 (1991).
26. Hashimoto, T., Todo, A., Itoi, H., and Kawai, H., *Macromolecules* **10,** 377 (1977).
27. Koberstein, J. T., Morra, B., and Stein, R. S., *J. Appl. Crystallogr*. **13,** 34 (1980).
28. Bacon, G. E., "Neutron Diffraction." Clarendon, Oxford, 1975.